Supplementary Information (SI) for ChemComm.
This journal is © The Royal Society of Chemistry 2024

Supplementary Information

Giant Molecule Acceptors Prepared by Metal-free Catalyzed Reactions towards Efficient Organic Solar Cells

*Siyuan Li[a], Zhilong He[a], Zhe Hao[a], Zhuping Fei[c] and Hongliang Zhong[a, b]**

[a] *School of Chemistry and Chemical Engineering, Shanghai Jiao Tong University, Shanghai 200240, China.*

[b] *Center for Advanced Low-dimension Materials, State Key Laboratory for Modification of Chemical Fibers and Polymer Materials, Donghua University, Shanghai 201620, China.*

[c] *Institute of Molecular Plus, Department of Chemistry, Key Laboratory of Organic Integrated Circuits, Ministry of Education &Tianjin Key Laboratory of Molecular Optoelectronic Science, Tianjin University, Tianjin 300072, China.*

1. General Procedure:

All reactions were carried out under an argon atmosphere. The solvents and reagents are used as commercially supplied, unless otherwise stated. ^{1}H NMR and ^{13}C NMR spectra were collected on a Bruker AV-400 (400 MHz) spectrometers. The residual solvent resonance of chloroform was used as an internal reference. Absorption spectra were measured by a PerkinElmer Lambda 750S recording

spectrophotometer. Cyclic voltammetry (CV) measurements of the target products were conducted on a CHI660D voltametric analyzer through conventional three-electrode configuration consisting of a platinum working electrode, a platinum wire counter electrode and an Ag/AgCl wire reference electrode in dichloromethane solution with 0.1 M tetrabutylammonium hexafluorophosphate (*n*-Bu_4NPF_6) as supporting electrolyte at room temperature.

2. Synthesis:

IDO was synthesized as reported by refs[1, 2].

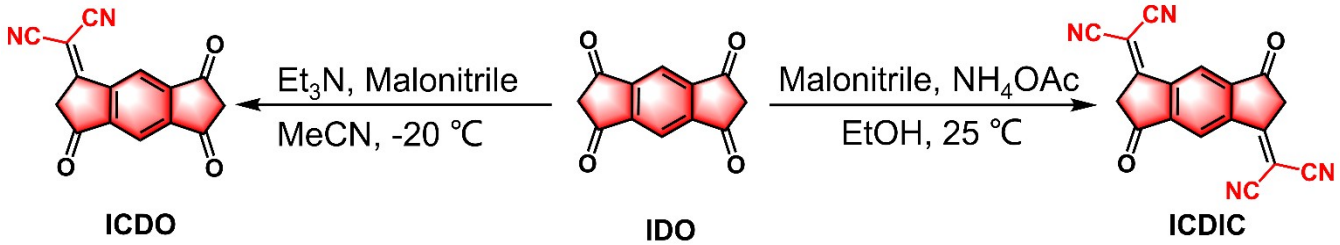

Scheme S1. The synthesis of ICDO and ICDIC.

ICDO: in an over dry flask, Et_3N (202 mg, 2.0 mmol) was added to the suspension of IDO (214 mg, 1.0 mmol) in MeCN (50 mL). The suspension changed to blue solution. After cooling to -20 ℃, the malononitrile (66 mg, 1.0 mmol) in MeCN (10 mL) was dropwise slowly. The reaction was stirred for 6 h, and then HCl (2M, 10 mL) was added. A brown precipitate was obtained by filtration. The precipitate was dissolved in MeCN, and then purified by column chromatography on silica gel with MeCN as the eluent to afford compound ICDO (178 mg, 0.68 mmol, 68% yield) as an orange solid. ^{1}H NMR (400 MHz, $CDCl_3$) δ 9.17 (s, 1H), 8.50 (s, 1H), 3.92 (d, J = 1.0 Hz, 2H), 3.47 (d, J = 1.0 Hz, 2H). ^{13}C NMR (101 MHz, $CDCl_3$) δ 207.86, 194.66, 194.52, 193.16, 163.49, 147.70, 146.84, 145.08, 121.11, 119.92, 111.33, 77.35, 77.03, 76.71, 46.10, 44.03.

ICDIC: IDO (214 mg, 1.0 mmol) was dispersed in EtOH (10 mL), then malononitrile (264 mg, 4.0 mmol)

and NH_4OAc (385 mg, 5.0 mmol) was added to the obtained deep blue suspension and the reaction mixture was left to stir for 2 h at room temperature. Water (100 mL) was added, and the solution was acidified till pH = 1 with a dropwise addition of concentrated HCl. The precipitate was collected by filtration and dissolved in ethyl acetate. The pure product was recrystallized using ethyl acetate/hexane to yield ICDIC as a brown powder (220 mg, 0.71 mmol, 71% yield). ^{1}H NMR (400 MHz, $CDCl_3$) δ 9.12 (s, 2H), 3.94 (s, 4H).

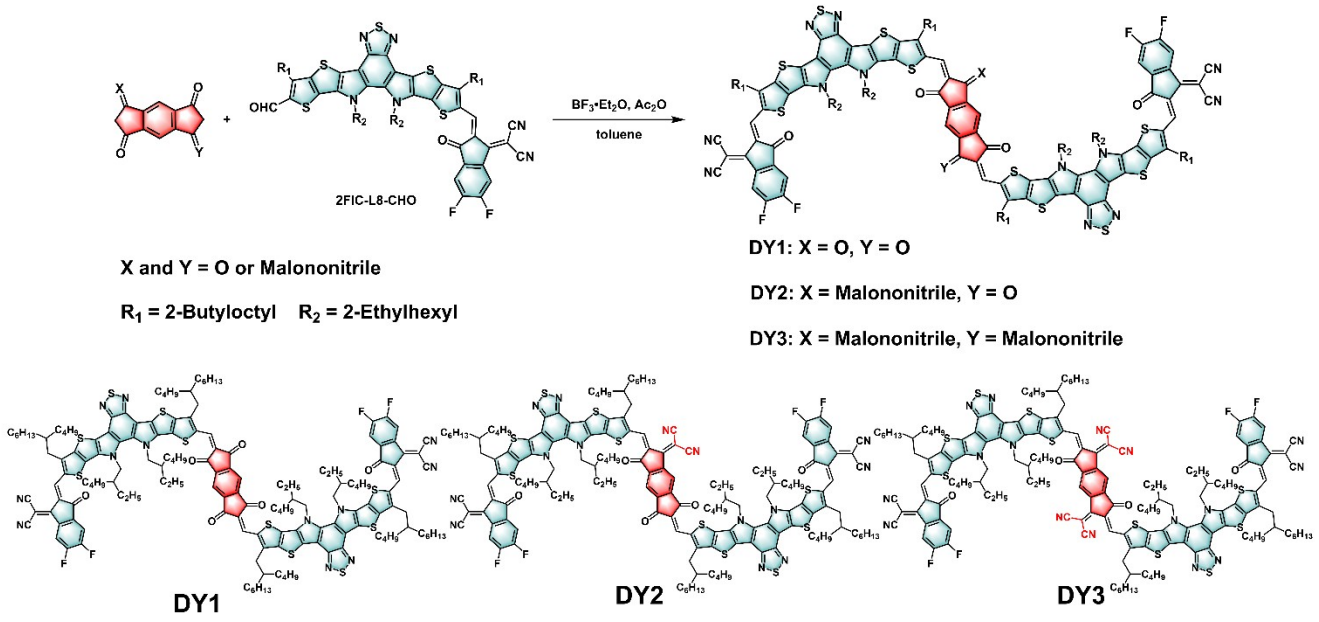

Scheme S2. Synthesis of DY1, DY2 and DY3.

DY1: IDO (12.2 mg, 0.057 mmol), compound 4 (152 mg, 0.12 mmol) were added into 10 mL toluene, after that acetic anhydride (0.1 mL) and BF_3•Et_2O (0.1 mL) were added to the flask. The reaction was performed at 60 °C for 10 min. The reaction droplets were added to methanol and crude DY1 was obtained by filtration. The crude DY1 was dissolved in a small amount of chloroform and purified by column chromatography on silica gel with dichloromethane/hexane (v/v, 1/1) as the eluent to afford pure DY1 (124.8 mg, 0.046 mmol, 76% yield) as a light brown solid. ^{1}H NMR (400 MHz, $CDCl_3$) δ 9.16 (s, 2H),

8.62-8.53 (m, 2H), 8.46 (m, 2H), 8.25 (m, 2H), 7.73 (m, 2H), 4.81 (s, 8H), 3.29-3.01 (m, 8H), 2.12 (m, 8H), 1.55–0.55 (m, 145H). ^{13}C NMR (101 MHz, $CDCl_3$) δ 201.00, 200.01, 192.46, 190.71, 164.03, 162.15, 159.82, 159.34, 158.70, 158.44, 155.94, 153.97, 153.04, 150.18, 147.57, 147.57, 145.03, 143.31, 141.73, 139.07, 137.16, 136.17, 134.59, 134.10, 133.46, 133.19, 129.62, 127.64, 127.23, 121.89, 119.81, 115.03, 113.66, 112.83, 108.79, 106.09, 105.74, 105.22, 101.45, 100.96, 97.49, 72.33, 71.15, 68.53, 64.09, 50.78, 39.17, 31.88, 31.60, 31.26, 30.86, 30.45, 29.85, 29.50, 29.47, 29.45, 29.31, 28.09, 22.86, 22.68, 22.48, 14.13, 14.03, 13.80. MS (MALDI-TOF) m/z: Calculated for [M^+] 2711.114; found: 2711.694.

DY2: ICDO (14.9 mg, 0.057 mmol), compound 4 (152 mg, 0.12 mmol) were added into 10 mL toluene, after that acetic anhydride (0.1 mL) and BF_3•Et_2O (0.1 mL) were added to the flask. The reaction was performed at 60 °C for 10 min. The reaction droplets were added to methanol and crude DY2 was obtained by filtration. The crude DY2 was dissolved in a small amount of chloroform and purified by column chromatography on silica gel with dichloromethane/hexane (v/v, 1/1) as the eluent to afford pure DY2 (121.5 mg, 0.044 mmol, 73% yiled) as a light brown solid. ^{1}H NMR (400 MHz, $CDCl_3$) δ 9.23-9.14 (m, 3H), 8.64-8.53 (m, 3H), 8.44 (m, 1H), 8.32 (m, 1H), 7.77-7.71 (m, 2H), 4.81 (s, 8H), 3.21 (s, 8H), 2.11 (s, 8H), 1.82–0.53 (m, 144H). ^{13}C NMR (101 MHz, $CDCl_3$) δ 203.60, 200.69, 194.40, 193.64, 188.83, 187.19, 156.97, 155.76, 151.78, 151.35, 150.06, 149.41, 149.28, 145.21, 144.48, 140.90, 140.45, 138.85, 135.46, 134.68, 133.45, 131.24, 130.56, 128.02, 126.63, 126.09, 115.78, 113.35, 113.06, 110.78, 110.45, 108.91, 106.82, 105.60, 105.11, 67.19, 65.96, 61.03, 60.87, 54.63, 54.34, 54.28, 39.34, 39.10, 36.27, 31.97, 31.82, 31.35, 29.97, 29.61, 29.43, 29.35, 24.56, 22.76, 22.63, 22.43, 14.10, 13.85, 13.79. MS (MALDI-TOF) m/z: Calculated for [M^+] 2760.131; found: 2760.414.

DY3: ICDIC (17.7 mg, 0.057 mmol), compound 4 (152 mg, 0.12 mmol) were added into 10 mL toluene,

after that acetic anhydride (0.1 mL) and BF_3•Et_2O (0.1 mL) were added to the flask. The reaction was performed at 60 °C for 10 min. The reaction droplets were added to methanol and crude DY3 was obtained by filtration. The crude DY3 was dissolved in a small amount of chloroform and purified by column chromatography on silica gel with dichloromethane/hexane (v/v, 1/1) as the eluent to afford pure DY3 (143.3 mg, 0.051 mmol, 85% yield) as a light black solid. ^{1}H NMR (400 MHz, $CDCl_3$) δ 9.16 (m, 4H), 8.58 (m, 4H), 7.77 (m, 2H), 5.09-4.64 (m, 8H), 3.24 (m, 8H), 2.34-1.96 (m, 8H), 1.40 (m, 144H). MS (MALDI-TOF) m/z: Calculated for [M^+] 2807.136; found: 2807.818.

3. Device fabrication and evaluations

Device fabrication

The patterned indium tin oxide glass (ITO) glass substrates (sheet resistance = 10 Ω sq^{-1}) were cleaned in detergent, deionized water, acetone, chloroform, acetone, and isopropanol sequentially by ultra-sonic bath for 15 min each and then dried by N_2 gas. Further UV-Ozone treatment for 10 min was applied before use. The PEDOT:PSS solution was spin-coated onto the cleaned ITO glass substrate at 3500 rpm of 45 s followed by annealing at 150 ℃ of 15 min in air. Then the PEDOT:PSS coated substrates were transferred into a nitrogen-filled glove box. Active layer materials were dissolved in chloroform at 60 ℃ at the donor concentration of 7.4 mg mL^{-1} with cinnamonitrile (CIN) as the additive. All solutions were stirred for 2 h in a nitrogen-filled glove box before spin-coating. The thermal annealing of active layer was carried out on the thermal platform with different temperature in a glove box. The fluorous solvent vapor annealing (FSVA) posttreatment of active layer was placed onto a stand in an airtight brown jar and the 200 μL perfluorotoluene was added into the jar, and the brown jar was put onto the hotplate with different temperature and time. Then PNDIT-F3N was dissolved in MeOH with the concentration of 0.55 mg mL^{-}

[1] as the electron transport layer was spin-coated on the active layer at 3500 rpm for 45 s. Finally, the anode, 100 nm Ag was deposited at a speed of 0.3 nm/s through a shadow mask by thermal evaporation in a vacuum chamber of under 2×10^{-6} Torr. The active area of each device was defined to 0.052 cm^2.

OSC device characterization

The device *J-V* characteristics were recorded by a Keithley 2420 Source Meter unit in forward direction under AM 1.5G 1 sun irradiance (100 mW•cm^{-2}) as generated by a 300W Xe lamp solar simulator (Enlitech SS-F5-3A) at room temperature. Standard Si diode with KG-5 filter was used to calibrate the light intensity. Enlitech EQE system (Enlitech QE-M110) with a Si diode as reference cell was used to characterize the EQE spectra. Monochromatic light was generated from an Enlitech lamp source with a monochromator.

Electron and hole mobility measurement

Hole-only diode configuration: ITO/PEDOT-PSS/blend films/MoO_3/Ag. PEDOT-PSS was spin-coated onto the ITO-glass substrate. Then the following layer was deposited by the same procedure as devices. Electron-only diode configuration: ITO/ZnO/blend films/PNDIT-F3N/Ag. The mobility in blend films was determined by fitting the dark current hole/electron-only diodes to the space-charge-limited current (SCLC) model. The mobility was determined by the eq. 1.

$$J = \frac{9\varepsilon_0\varepsilon_r\mu_0 V^2}{8L^3} \quad \text{(eq. 1)}$$

where J is current density, μ_0 is the hole or electron mobility, ε_r is the dielectric permittivity of the active layer (generally taken to be about 3 for organic materials), ε_0 is the dielectric permittivity of free space ($\varepsilon_0 = 8.854\times10^{-12}$ F/m), L is the film thickness, and V is the voltage, which is defined as $V = V_{appl} - V_{bi}$,

where V_{appl} is the applied voltage, V_{bi} is the built-in voltage which is related to the difference in the work function of the electrodes.

Table S1 Summary of SC and correlation indexes of representative acceptors and donor.

Material	NSS	RY	NUO	NCC	NHC	SC	Refs.
Y6	15	96.15	26	6	25	54.42	2
EV-i	23	529.65	37	12	33	80.54	3
GT-I	38	589.80	41	16	33	100	4
PM6	14	68.49	20	7	22	50.01	5
PF7	10	27.17	19	6	23	41.69	6
DY1	19	86.96	34	12	29	67.47	This work
DY2	20	133.86	35	13	29	71.39	This work
DY3	20	110.13	35	12	29	70.63	This work

Synthetic complexity (SC): The synthetic complexity analysis is calculated through the reported mothed.[5-7]

$$SC = 35\frac{NSS}{NSS_{max}} + 25\frac{log(RY)}{log(RY_{max})} + 15\frac{NUO}{NUO_{max}} + 15\frac{NCC}{NCC_{max}} + 10\frac{NHC}{NHC_{max}} \quad \text{(eq. 1)}$$

Where NSS is the number of synthetic steps, RY is the reciprocity yields, NUO is the number of unit operations required for the isolation/purification, NCC is the number of column chromatography, NHC is the number of hazardous chemicals used for their preparation, and NSS_{max}, RY_{max}, NUO_{max}, NCC_{max}, and NHC_{max} are the maximum values of the corresponding parameters.

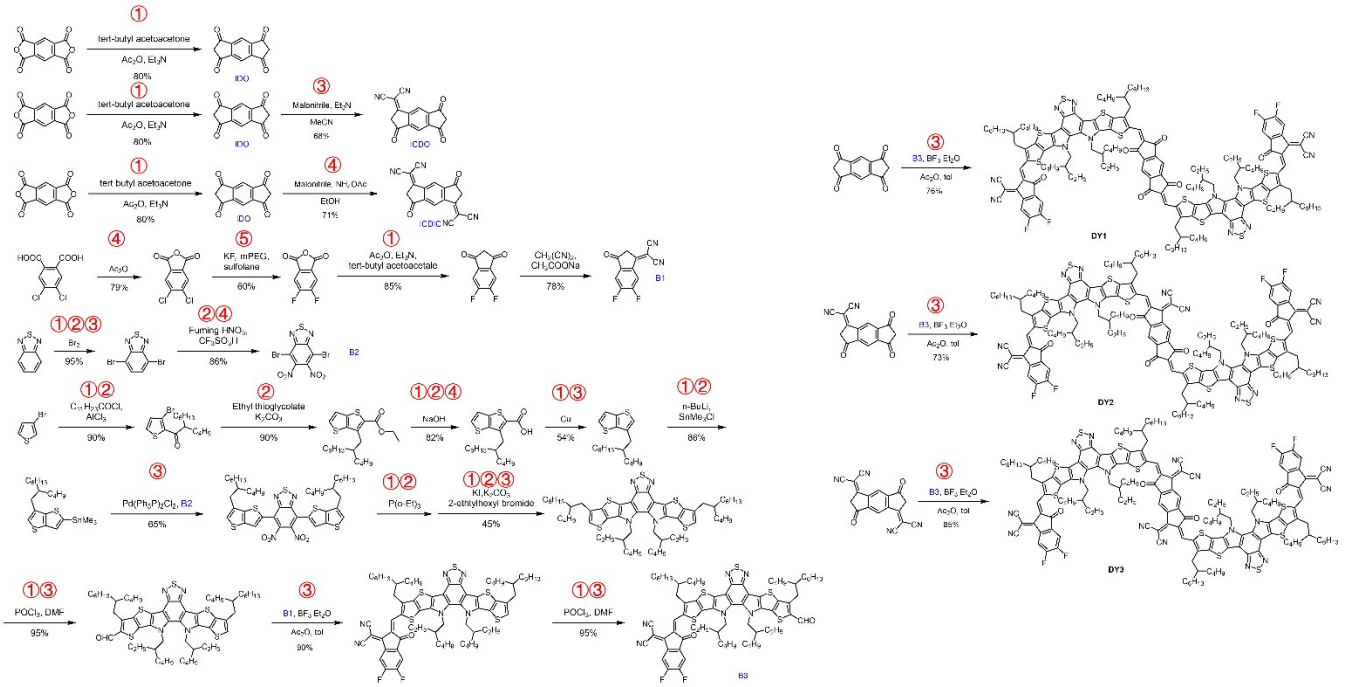

Scheme S1 Synthetic complexity of DY1, DY2 and DY3. The unit operations are represented by codes: 1 = quenching/neutralization, 2 = extraction, 3 = column chromatography, 4 = recrystallization, 5 = distillation/sublimation.

Table S2 Optical and electrochemical properties of the acceptor materials.

Sample	λ_{max}^{sol} (nm)	$\varepsilon_{sol.}$ ($M^{-1}cm^{-1}$)	λ_{max}^{film} (nm)	λ_{edge} (nm)	E_g^{opt} (eV)	LUMO (eV)	HOMO (eV)
DY1	742	3.45	778	851	1.46	-3.89	-5.56
DY2	795	4.14	830	919	1.35	-4.06	-5.66
DY3	819	4.47	872	995	1.24	-4.21	-5.67

Table S3 Device parameters of the OSCs with different DY2 ratios under AM 1.5G irradiation at 100 mW cm^{-2}.

PF7:DY2	V_{oc} (V)	J_{sc} (mA cm^{-2})	*FF* (%)	PCE (%)
1 : 1	0.831	23.46	62.62	12.21
1 : 1.1	0.854	24.40	67.04	13.97
1 : 1.2	0.842	23.13	63.90	12.44

Table S4 Device parameters of the OSCs based on PF7:DY2 with different additive concentrations under AM 1.5G irradiation at 100 mW cm^{-2}.

CIN (v/v)	V_{oc} (V)	J_{sc} (mA cm^{-2})	*FF* (%)	PCE (%)
0.3 %	0.862	24.66	72.12	15.33
0.5 %	0.856	24.33	73.97	15.40
1.0 %	0.835	23.68	68.56	13.42

Table S5 Device parameters of the OSCs based on PF7:DY2 with different temperature and time of TA and FSVA under AM 1.5G irradiation at 100 mW cm^{-2}.

Treatment	Time (min)	V_{oc} (V)	J_{sc} (mA cm^{-2})	*FF* (%)	PCE (%)
TA 80 ℃	10	0.842	24.84	66.56	13.92
TA 90 ℃	7	0.837	24.64	66.56	13.73
TA 100 ℃	5	0.835	25.17	65.70	13.97
FSVA 80 ℃	10	0.851	25.60	70.99	15.44
FSVA 80 ℃	15	0.854	25.80	73.69	16.23
FSVA 90 ℃	7	0.847	25.51	72.11	15.58
FSVA 100 ℃	5	0.845	25.80	71.65	15.62

Table S6 Contact angle of measurement parameters and surface energy for PF7, DY1, DY2, and DY3 neat films.

Sample	H_2O (°)	EG (°)	γ^{total} (mN m^{-1})
PF7	104.4	81.3	19.68
DY1	86.4	71.3	21.35
DY2	87.5	66.9	23.12
DY3	92.2	65.0	26.21

Contact angle measurement and surface energy calculation

The interfacial tension between water (A) and ethylene glycol (B) is calculated through the Wu's model.[8]

$$\gamma_A(1+cos\theta_A) = \frac{4\gamma_A^d\gamma_s^d}{\gamma_A^d+\gamma_s^d} + \frac{4\gamma_A^p\gamma_s^p}{\gamma_A^p+\gamma_s^p} \quad \text{(eq.2)}$$

$$\gamma_B(1+cos\theta_B) = \frac{4\gamma_B^d\gamma_s^d}{\gamma_B^d+\gamma_s^d} + \frac{4\gamma_B^p\gamma_s^p}{\gamma_B^p+\gamma_s^p} \quad \text{(eq. 3)}$$

$$\gamma^{total} = \gamma^d + \gamma^p \quad \text{(eq. 4)}$$

$$\chi^{D-A} = k\,(\sqrt{\gamma^D} - \sqrt{\gamma^A})^2 \quad \text{(eq. 5)}$$

The γ_A and γ_B were the surface energy of water and ethylene glycol respectively. and γ^d and γ^p are the dispersion and polar components of γ^{total}, θ is the droplet contact angle on the film. The Flory-Huggins interaction parameter between the donor (D) and the acceptor (A) is calculated through eq. 5.

Table S7 GIWAXS parameters of neat films and blend films.

Sample	OOP (010)			
	q (Å^{-1})	$d_{\pi\text{-}\pi}$ (Å)	FWHM	CCL
DY1	1.69	3.72	0.276	20.49
DY2	1.71	3.67	0.249	22.71
DY3	1.73	3.63	0.238	23.76
PF7:DY1	1.71	3.67	0.352	16.07
PF7:DY2	1.72	3.64	0.287	19.68
PF7:DY3	1.71	3.67	0.262	21.58

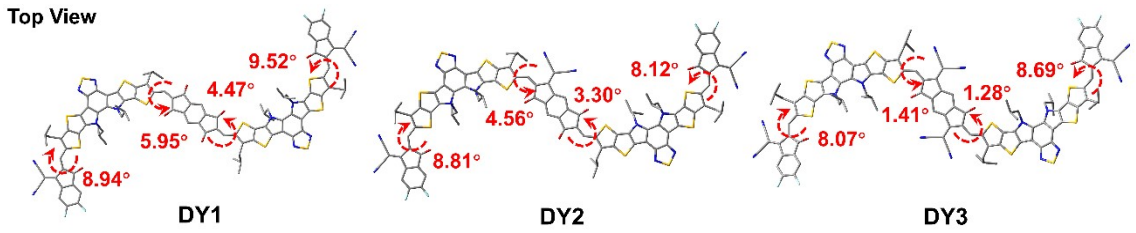

Fig. S1 Optimized conformational geometries for DY1, DY2 and DY3.

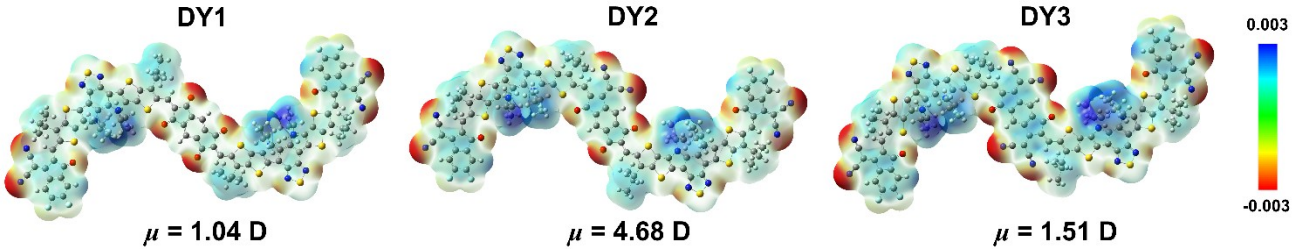

Fig. S2 Electrostatic potential distribution of DY1, DY2 and DY3.

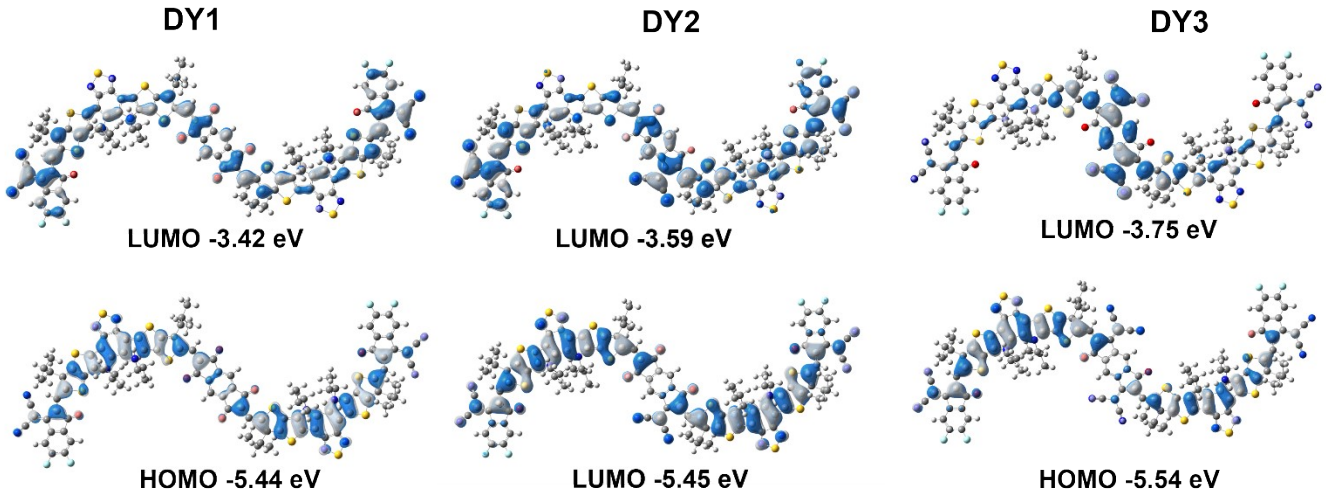

Fig. S3 Molecular orbitals of the simplified molecular models for DY1, DY2 and DY3.

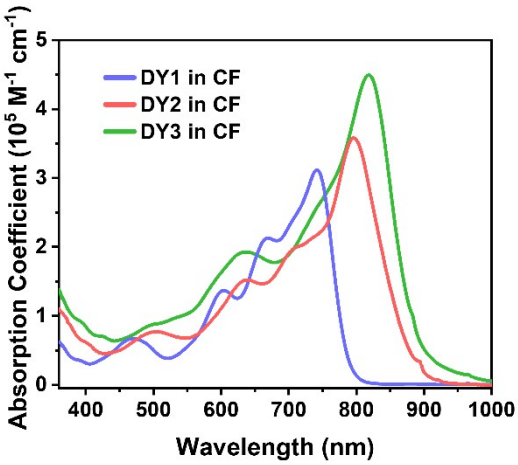

Fig. S4 Absorption spectra with extinction coefficients in chloroform solutions of DY1, DY2 and DY3.

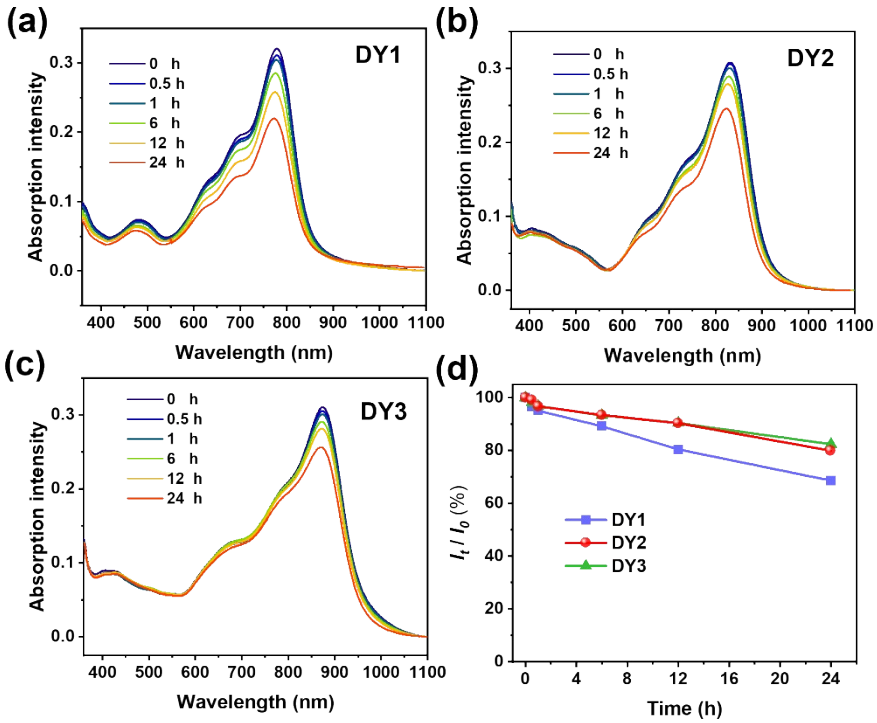

Fig. S5 Photostability of (a) DY1, (b) DY2 and (c) DY3 neat films under AM 1.5G (100 mW cm^{-2}) irradiation for 24 h. (d) Maximum absorption peak intensity ratio I_t/I_0 versus irradiation time.

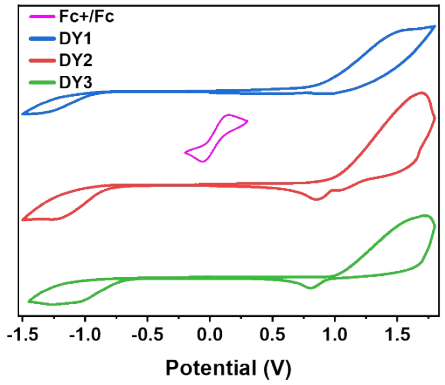

Fig. S6 Cyclic voltammetry curves of DY1, DY2 and DY3.

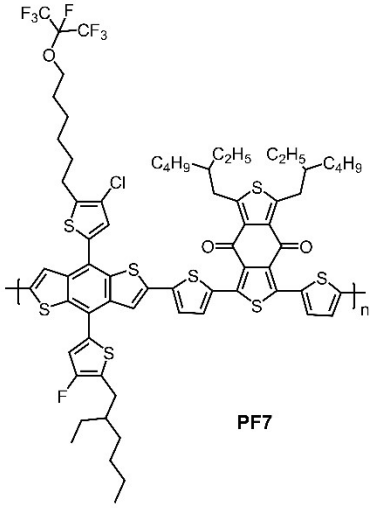

Fig. S7 Chemical structure of PF7.

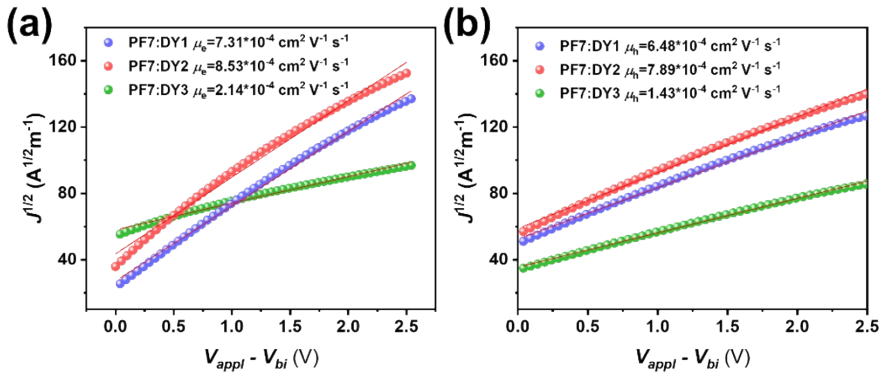

Fig. S8 Electron mobility (a) and hole mobility (b) of PF7:DY1, PF7:DY2 and PF7:DY3.

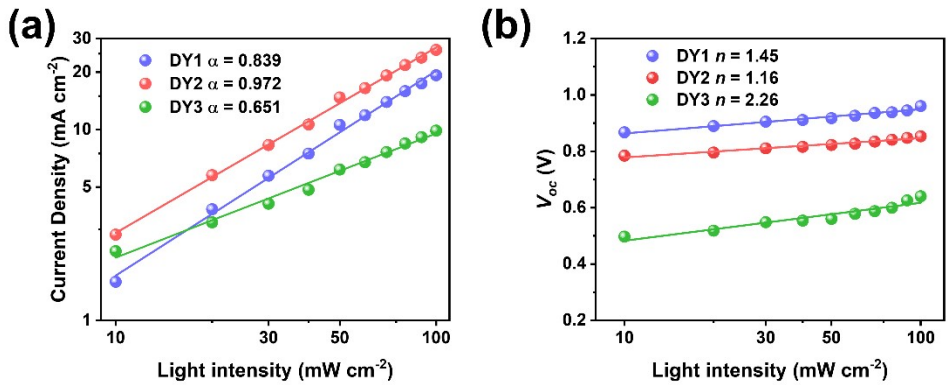

Fig. S9 (a) J_{sc} and (b) V_{oc} versus P_{light} characteristics of optimized OSCs based on PF7:DY1, PF7:DY2 and PF7:DY3.

As shown in Fig. S9, the slopes of the J_{sc} versus light intensity curve (α) are determined to be 0.839, 0.972, and 0.651 for DY1-, DY2-, and DY3-based solar cells, respectively. The corresponding n values determined with the slopes for PF7:DY1, PF7:DY2, and PF7:DY3-based devices are 1.45 *kT/q*, 1.16 *kT/q*, and 2.26 *kT/q*, respectively. The α value and the n value based on PF7:DY2 device exhibits the closest to 1 than other ones, suggesting the successful suppression of the bimolecular and trap-assisted recombination in DY2-based device. As for the DY3-based device, the poor morphology renders the values of α and n have deviated from the normal range, indicating that the charge undergoes severe recombination in the device and then resulting in the rather low V_{oc} and J_{sc}.

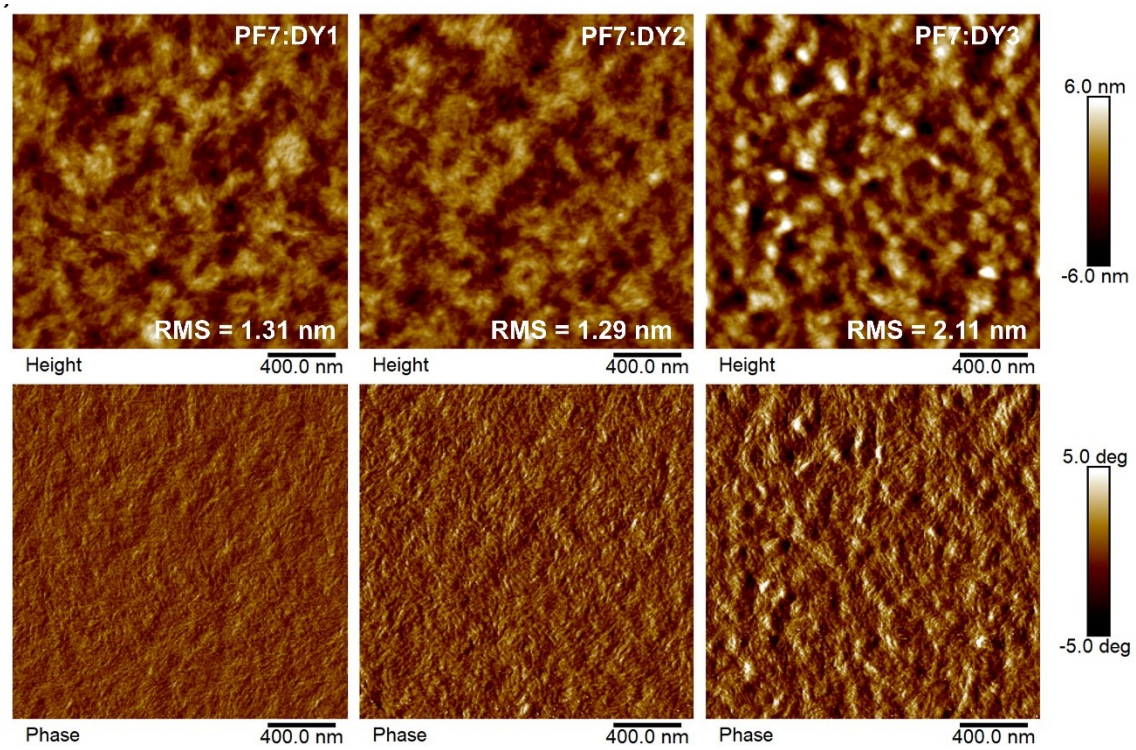

Fig. S10 AFM high (top) and phase (bottom) images of PF7:DY1, PF7:DY2 and PF7:DY3 blend films.

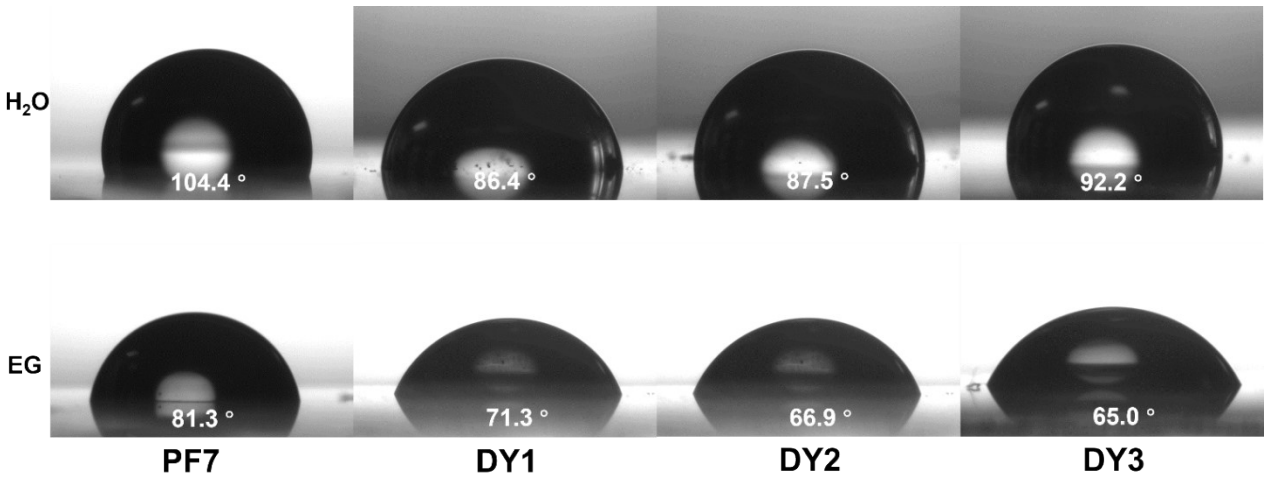

Fig. S11 Photographs of water and ethylene glycol (EG) droplets on the top surfaces of PF7, DY1, DY2 and DY3 neat films.

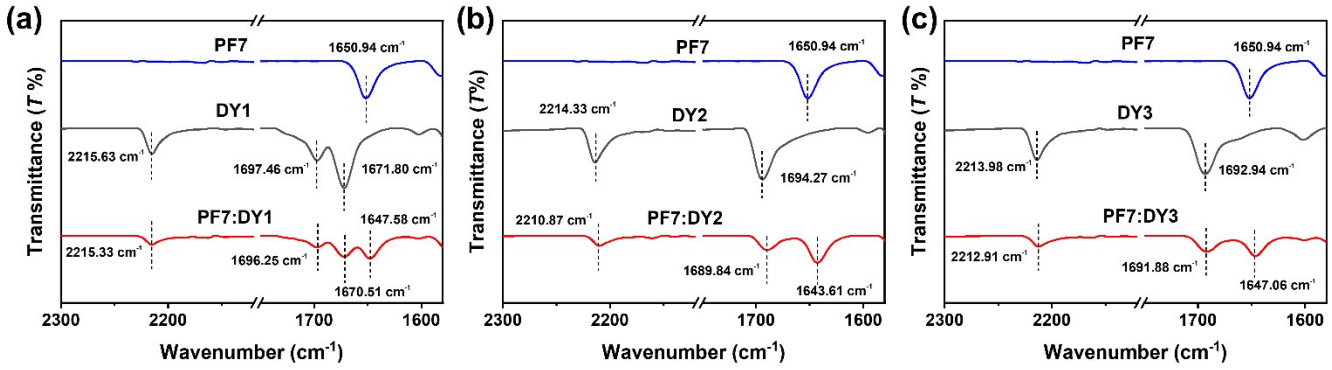

Fig. S12 FTIR spectra of (a) PF7, DY1 and PF7:DY1 film, (b) PF7, DY2 and PF7:DY2 film, (c) PF7, DY3 and PF7:DY3 film.

The peak at 1650.94 cm^{-1} is assigned to the *C=O* stretching in neat PF7 film. The *C=O* stretching peaks located at 1671.80 cm^{-1} and 1697.46 cm^{-1} for DY1, 1694.27 cm^{-1} for DY2 and 1692.94 cm^{-1} for DY3. Compared with the neat PF7 and GMAs, PF7:DY1, PF7:DY2 and PF7:DY3 blends exhibit obvious shifts, moving into low wavenumber, from 1650.94 to 1647.58, 1643.61 and 1647.06 cm^{-1}, respectively. At the same time, the peaks at 2215.63, 2214.33 and 2213.98 cm^{-1} are assigned to -*C*≡*N* stretching in DY1, DY2 and DY3, respectively. While the GMAs are blended with PF7, the -*C*≡*N* stretching peaks also move to low wavenumber, from 2215.63 to 2215.33 cm^{-1} for DY1 based film, 2214.33 to 2210.87 cm^{-1} for DY2 based film, and 2213.98 to 2212.91 cm^{-1} for DY3 based film, respectively. The shift of vibration peaks could contribute to the interaction between GMAs and PF7. Among the three GMAs, PF7:DY2 blend film has the largest vibration shifts, implying the strongest interaction is formed between PF7 and DY2, which originates from the large dipole moment of DY2.

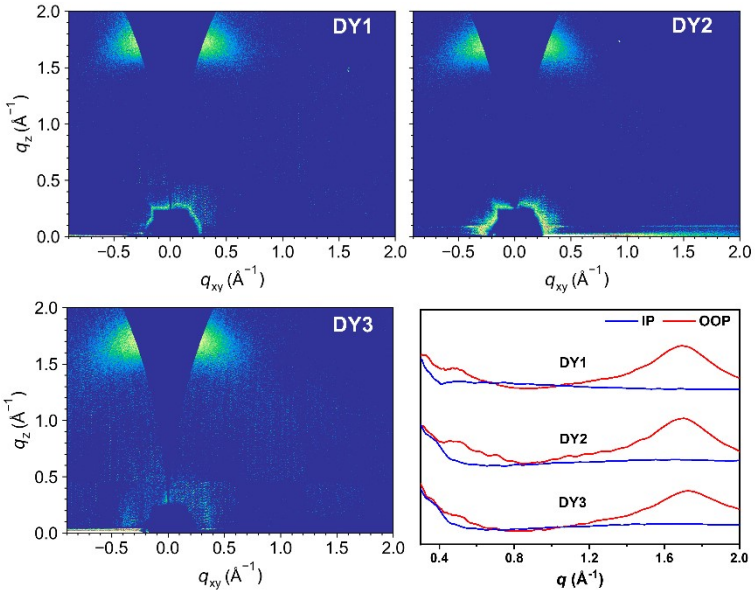

Fig. S13 2D GIWAXS patterns and corresponding in-plane and out-of-plane line-cut profiles for DY1, DY2 and DY3.

As depicted in Fig. S13 and Table S7, all neat films show enhanced (010) diffraction peaks in out-of-plane (OOP) direction. The (010) diffraction peaks of DY1, DY2 and DY3 neat films are located at 1.69 Å^{-1}, 1.71 Å^{-1}, and 1.73 Å^{-1}, respectively, with the comparative π-π stacking distance (dπ-π) of 3.71 Å, 3.67 Å and 3.63 Å, respectively, suggesting predominant face-on orientation. The calculated crystallite coherence length (CCL) values of (010) diffraction peaks are 20.49 Å for DY1, 22.71 Å for DY2 and 23.76 Å for DY3, respectively. These results demonstrate that the stacking distance of three GMAs decreases, and the crystallization capacity improves with an increasing number of malononitrile substituents on the linker units, owing to the powerful coplanarity of the malononitrile and enhanced conjugation between BTP core fragments and dual-functional linker blocks.

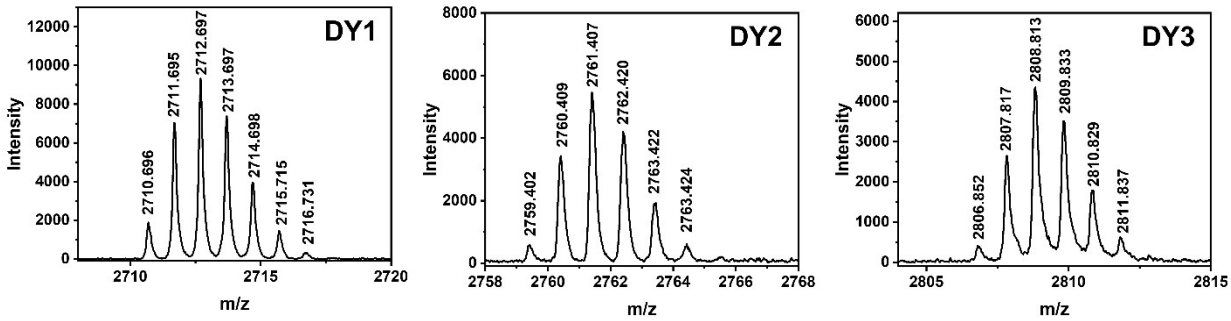

Fig. S14 Mass spectra (MALDI-TOF) of DY1, DY2 and DY3.

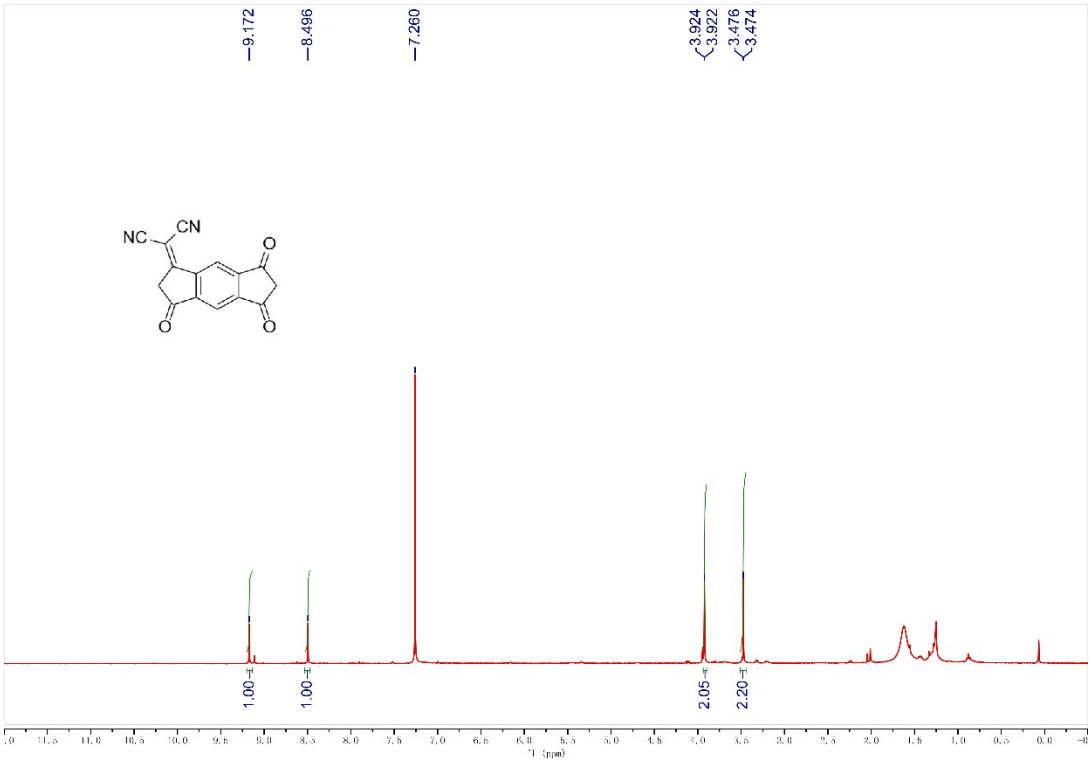

Fig. S15 ^{1}H NMR spectrum of ICDO.

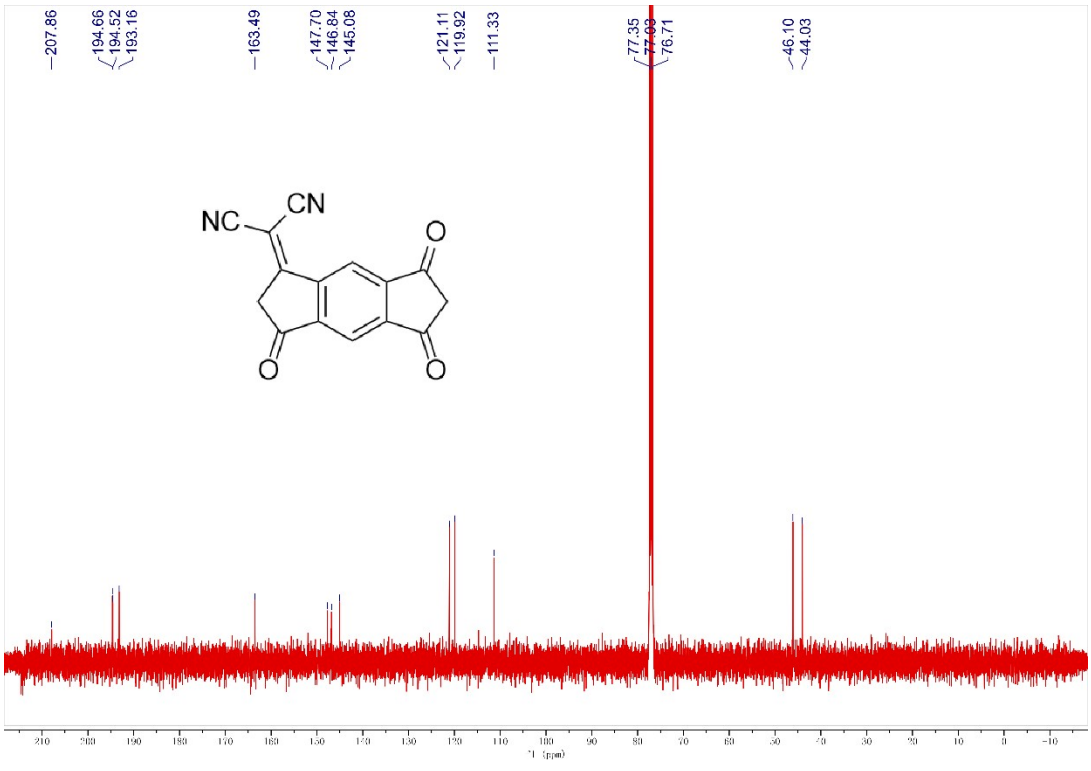

Fig. S16 ^{13}C NMR spectrum of ICDO.

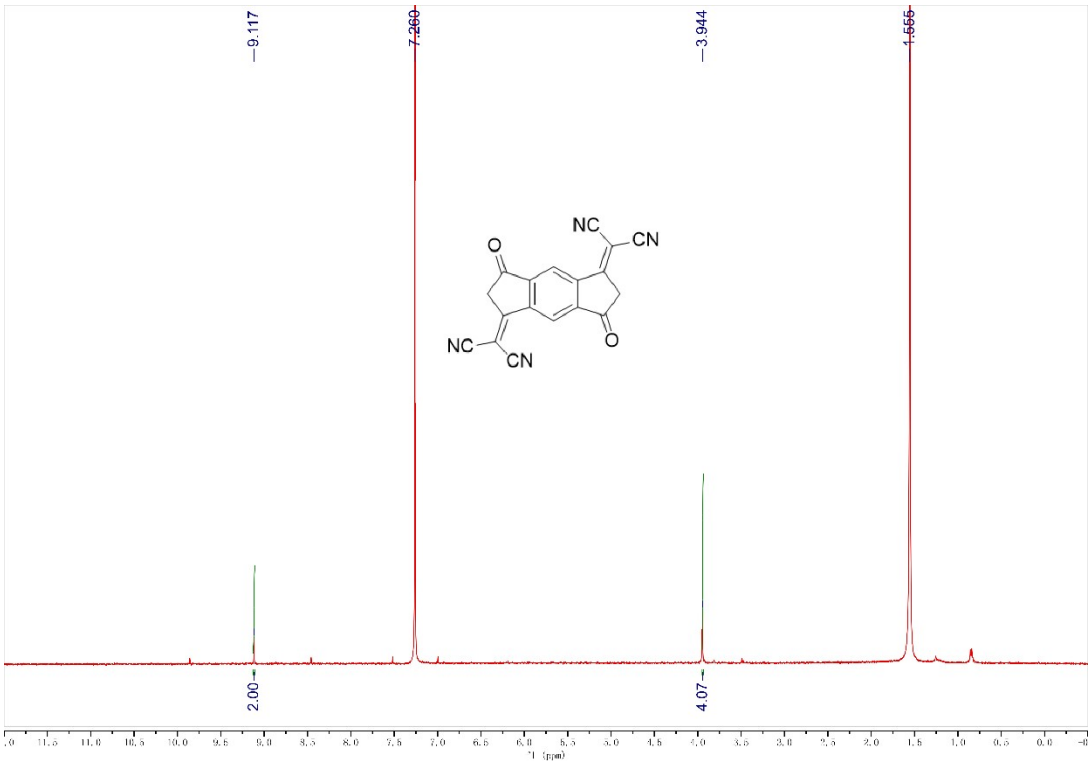

Fig. S17 ^{1}H NMR spectrum of ICDCI.

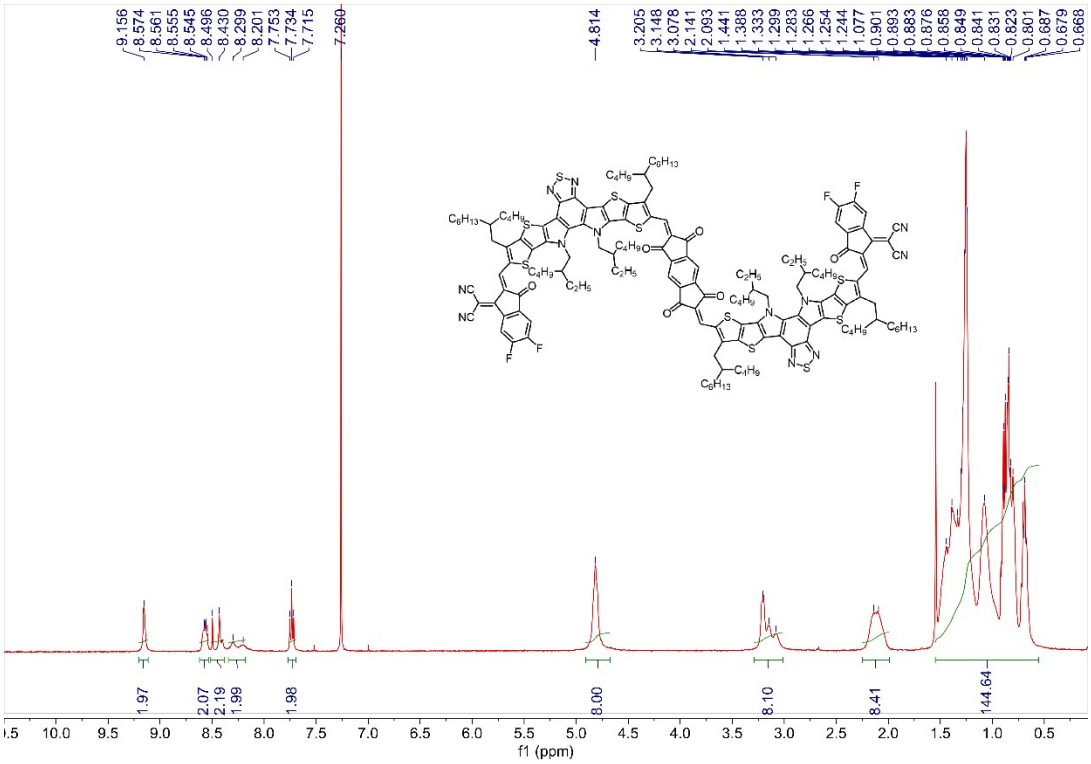

Fig. S18 ^{1}H NMR spectrum of DY1.

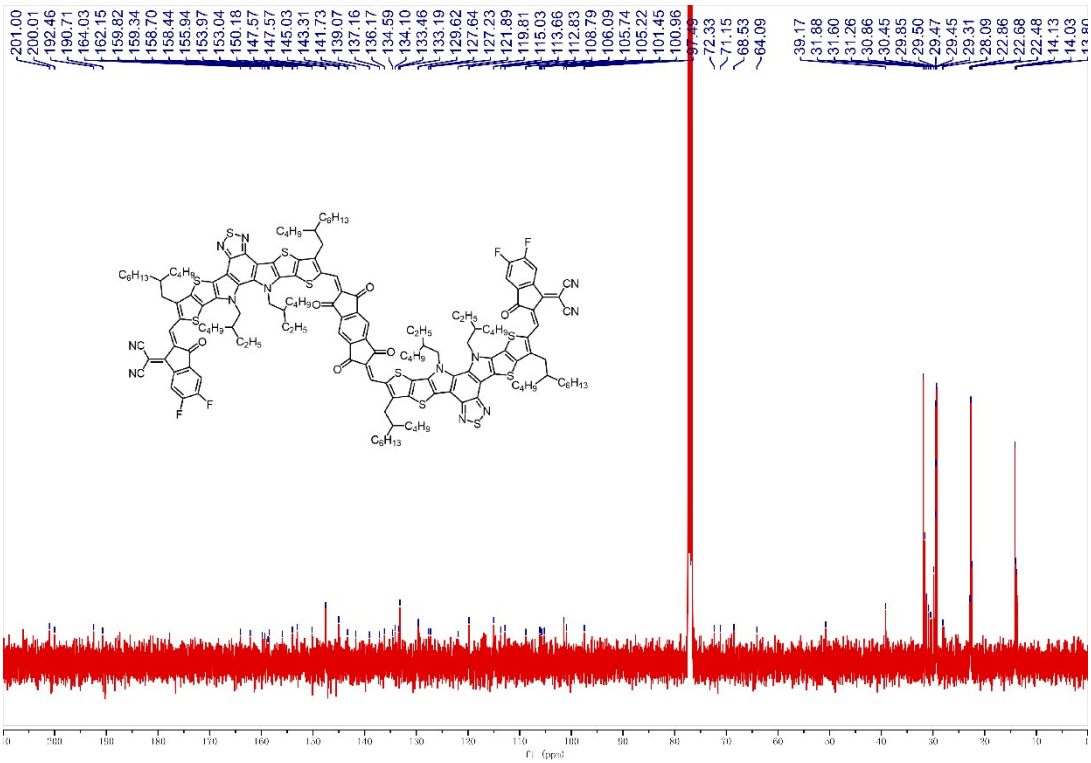

Fig. S19 ^{13}C NMR spectrum of DY1.

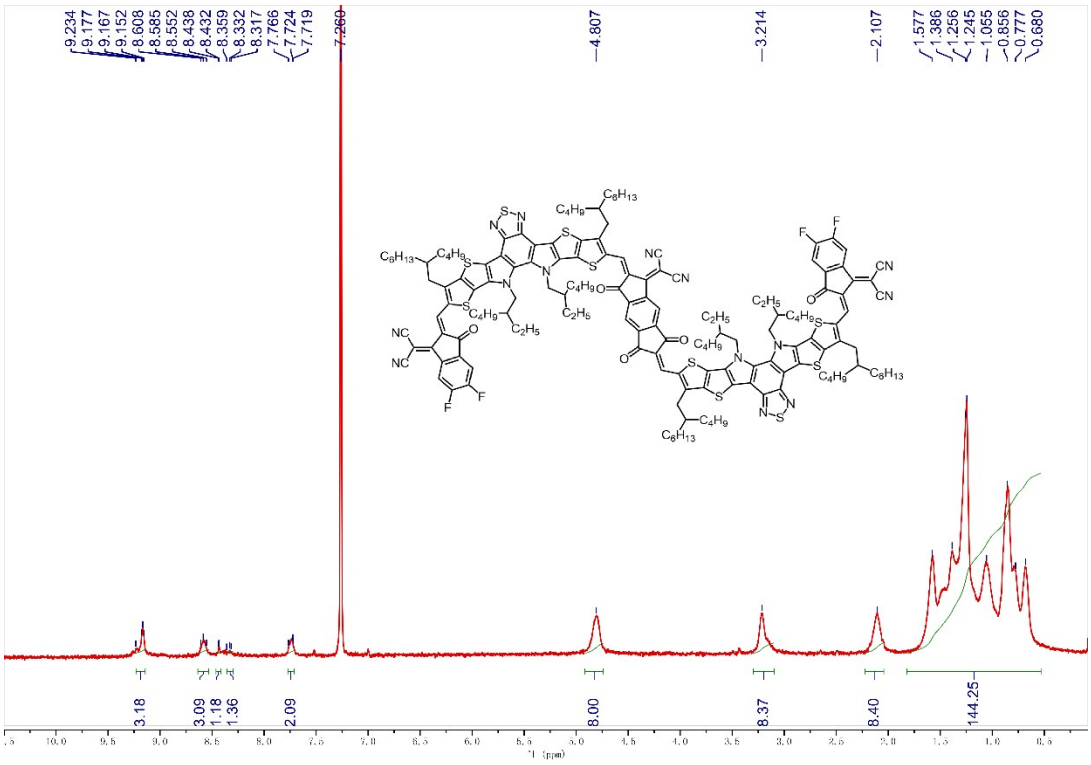

Fig. S20 ^{1}H NMR spectrum of DY2.

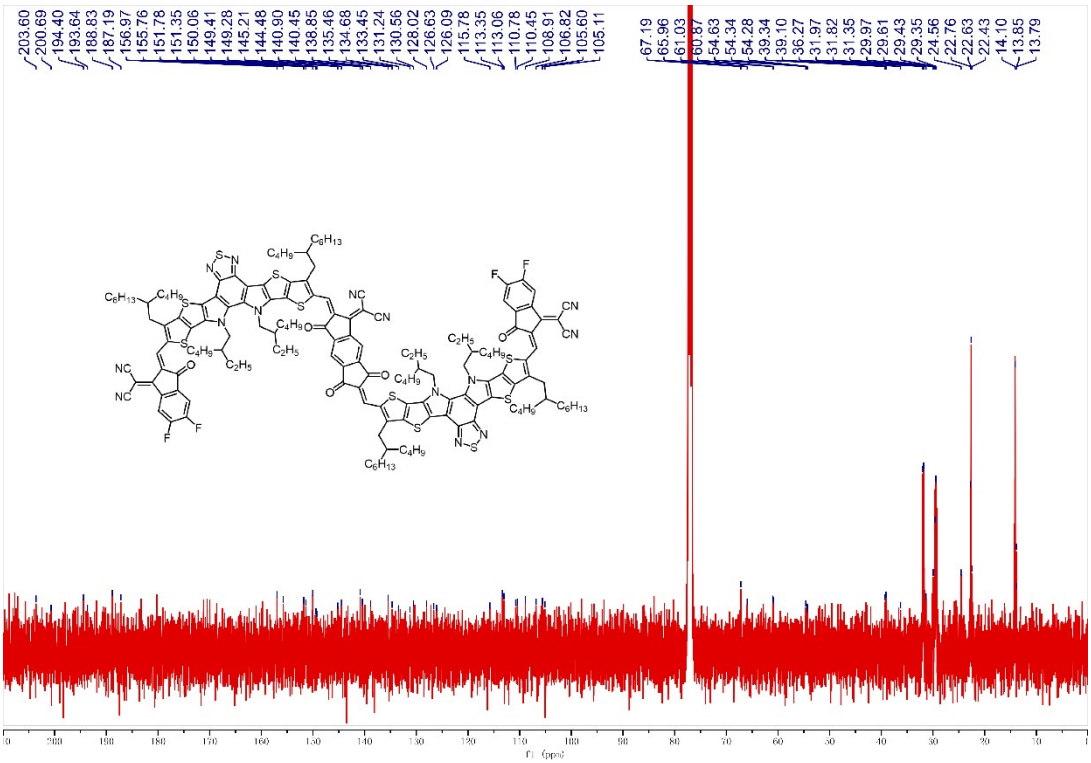

Fig. S21 ^{13}C NMR spectrum of DY2.

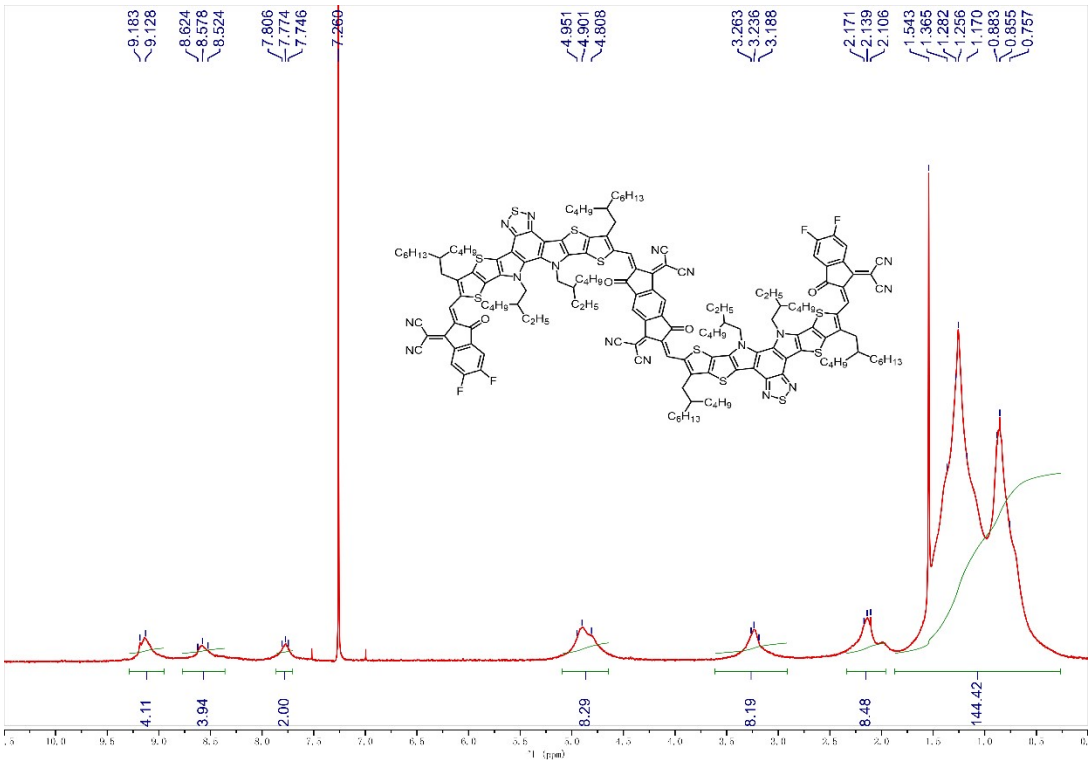

Fig. S22 ^{1}H NMR spectrum of DY3.

References:

(1) Zagata, A.; Traskovskis, K.; Belyakov, S.; Mihailovs, I.; Bundulis, A.; Rutkis, M. Dicyanomethylene-functionalized S-indacene-based D-π-A-π-D Dyes Exhibiting Large Near-infrared Two-photon Absorption Cross-section. *Dyes Pigments* **2023**, *208*, 110864.

(2) Githaiga, G. W.; Woodward, A. W.; Morales, A. R.; Bondar, M. V.; Belfield, K. D. Photophysical and Computational Analysis of a Symmetrical Fluorene-Based Janus Dione Derivative. *J. Phys. Chem. C* **2015**, *119* (36), 21053-21059.

(3) Zhuo, H.; Li, X.; Zhang, J.; Qin, S.; Guo, J.; Zhou, R.; Jiang, X.; Wu, X.; Chen, Z.; Li, J.; Meng, L.; Li, Y. Giant Molecule Acceptor Enables Highly Efficient Organic Solar Cells Processed Using Non-halogenated Solvent. *Angew. Chem. Int. Ed.* **2023**, *62* (26), e202303551.

(4) Zhuo, H.; Li, X.; Qin, S.; Zhang, J.; Gong, Y.; Wu, Y.; Zou, T.; Chen, Z.; Yin, K.; Yuan, M.; Li, J.; Meng, L.; Li, Y. Effect of Molecular Conformation on Intermolecular Interactions and Photovoltaic Performances of Giant Molecule Acceptors. *Adv. Funct. Mater.* **2024**, 2410092.

(5) Yang, W.; Wang, W.; Wang, Y.; Sun, R.; Guo, J.; Li, H.; Shi, M.; Guo, J.; Wu, Y.; Wang, T.; Lu, G.; Brabec, C. J.; Li, Y.; Min, J. Balancing the efficiency, stability, and cost potential for organic solar cells

via a new figure of merit. *Joule* **2021**, *5* (5), 1209-1230.
(6) Yang, Q.; Chen, H.; Lv, J.; Huang, P.; Han, D.; Deng, W.; Sun, K.; Kumar, M.; Chung, S.; Cho, K.; Hu, D.; Dong, H.; Shao, L.; Zhao, F.; Xiao, Z.; Kan, Z.; Lu, S. Balancing the Efficiency and Synthetic Accessibility of Organic Solar Cells with Isomeric Acceptor Engineering. *Adv. Sci.* **2023**, *10* (20), 2207678.
(7) Guo, J.; Qiu, B.; Yang, D.; Zhu, C.; Zhou, L.; Su, C.; Jeng, U.-S.; Xia, X.; Lu, X.; Meng, L.; Zhang, Z.; Li, Y. 15.71% Efficiency All-Small-Molecule Organic Solar Cells Based on Low-Cost Synthesized Donor Molecules. *Adv. Funct. Mater.* **2022**, *32* (13), 2110159.
(8) Wu, S. Polar and Nonpolar Interactions in Adhesion. *J. Adhes.* **1973**, *5* (1), 39-55.